View metadata, citation and similar papers at core.ac.uk
brought to you by CORE
provided by Ghent University Academic Bibliography

Structure of F_2^- centers in K_2YF_5 and their relation to thermoluminescence below room temperature

D. G. Zverev, H. Vrielinck[§], P.F. Smet[§], D. Poelman and F. Callens

Department of Solid State Sciences, Ghent University

Krijgslaan 281-S1, B-9000 Gent, Belgium

[§]Postdoctoral fellow of the Flemish Research Foundation (FWO-Vlaanderen)

Submission date 26.02.2009

ABSTRACT

X-ray irradiation at 77K produces signals from several trapped hole and/or electron centers in the electron paramagnetic resonance (EPR) spectra of rare-earth doped K_2YF_5. Five of the spectral components have a structure typical of a center with electron spin **S=½** exhibiting a strong hyperfine interaction with two nearly equivalent ^{19}F nuclei. They are identified as V- or H-type intrinsic trapped hole centers, having the F_2^- molecular anion as their core. Three centers are characterized by monoclinic *g* and ^{19}F self hyperfine tensors, i.e. with one principal axis along the crystal's twofold screw axis, the two others are triclinic. Plausible models for these five centers are discussed and via thermal annealing experiments, in which EPR and thermoluminescence (TL) spectra are simultaneously monitored, their role in the TL processes below room temperature is investigated.

I. INTRODUCTION

Recently rare-earth (RE) doped K_2YF_5 crystals have received considerable attention because when activated by Ce^{3+}, Pr^{3+}, Dy^{3+}, Tb^{3+} or Tm^{3+}, these crystals exhibit strong visible thermoluminescence (TL) after exposure to different types of ionizing radiation (α, β, γ, or X-rays). Therefore, they are promising for applications in new sensitive radiation detectors. Quite a few recent papers are devoted to the TL response and the unraveling of its origin.[1-7] The possibility of using such crystals as scintillators has been explored as well.[8-10]

In the latter context it has been discovered that for some RE activators the shape of the TL glow curve depends on the type of radiation[2] and pre-sensitisation treatments (irradiation with γ rays),[6] offering possibilities to discriminate mixed radiation fields. These findings indicate that exposure of the crystals to ionizing radiation produces various types of radiation defects with different thermal stabilities and which may be preferentially formed depending on the specific exposure conditions. Moreover, in a number of these studies it has been suggested that the RE dopant ions may, next to their role as an activator, also act as a carrier trapping center. Identification of radiation defects in these crystals – and in particular the trapped electron and hole centers involved in the TL processes – is thus important for understanding and

controlling these effects. Electron paramagnetic resonance (EPR), electron nuclear double resonance (ENDOR) are the spectroscopic methods of choice for determining the microstructure of radiation defects in these materials, which are very often paramagnetic, and in principle also allow to detect changes in the valence state of the RE ions. From EPR and ENDOR experiments *g* and hyperfine (HF) *A* tensors are determined, which give information about the symmetry and lattice position of the centers and neighboring ions.[11, pp.141-154] In addition, monitoring the intensity of the EPR signals after thermal bleaching may reveal the role of these defects in TL processes.[12, 13]

In order to fully exploit the possibilities of EPR and ENDOR, one has to know the symmetry of the undisturbed lattice in detail. To this end, we recently studied the angular dependence of the EPR spectrum for Gd^{3+} impurities and Ce^{3+} dopant ions in K_2YF_5, and established that the Y^{3+} site has mirror (C_h) symmetry. Hence the crystal's space group was shown to be *Pnam*, (number 63)[14] and not *Pna2₁*, as suggested from X-ray diffraction.[15, 16] This implies that the YF_7 polyhedra have a horizontal mirror plane (parallel to the *ab* plane), containing the Y^{3+} and three F^- ligand ions. The corresponding site symmetry is monoclinic (C_h), whereas all other substitutional lattice positions have triclinic C_1 symmetry.

In an initial study of the radiation defects in $K_2YF_5:Ce^{3+}$ crystals, a semi-quantitative relation between the thermal bleaching of EPR spectra and the occurrence of TL peaks could be established.[17, 18] At least four distinct radiation-induced centers were detected after X-ray irradiation at room temperature (300K) and were labeled C1 – C4, in order of decreasing thermal stability. The most stable center, C1, was recently identified as an oxygen-related (molecular) anion replacing a lattice F^-.[18] The least stable center, C4, with a lifetime of approximately two hours at 300K, could readily be identified as an F_2^--type intrinsic trapped hole center, based on its strong HF interaction with two ^{19}F nuclei. The present paper is devoted to a thorough study of this type of centers, produced in K_2YF_5 doped with Ce or Tb after X-ray irradiation at 77K. Five types of F_2^- centers are clearly distinguished. From a detailed analysis of the *g*-tensor and HF interactions, the structure and lattice location of the two most stable centers can be determined. Additionally the correlation between thermal bleaching of these centers and the TL below 300K is investigated and preliminary explanations for the occurrence for certain glow peaks are presented.

II. CRYSTAL GROWTH AND EXPERIMENTAL SETUP

K_2YF_5 crystals were hydrothermally synthesized at the Institute of General and Inorganic Chemistry of the Russian Academy of Sciences in Moscow (N. M. Khaidukov) as described earlier.[2, 19] Crystals with close to stoichiometric composition are expected to be obtained in this way. This is confirmed by the analysis of the EPR spectra of the RE^{3+} dopants and impurities in these crystals, which clearly shows that only one type of Y^{3+} sites is available. However, due to the specific growth conditions (from aqueous

solution) and the similarity between hydroxyl and fluoride ions, the concentration of OH^- ions, substitutionally incorporated on F^- positions, may be substantial.[20-22] Carrier trapping at such common impurity ions may be the origin of several paramagnetic centers observed in various doped and undoped crystals after irradiation at room temperature, among which the C1 center[18] (see above).

The crystals were cut to approximate 1.4×1.4×2 mm^3 dimensions with a diamond wire saw, the long edge corresponding to the crystallographic *a*, *b* or *c* axis, and mounted on a quartz rod (2 mm diameter) allowing for sample rotation in the magnetic field. The crystal orientation was initially controlled by X-ray diffraction and definitively determined during the fitting of the experimental data. The misalignments of the rotation planes (*ab, ac, bc*) could be determined with an accuracy of 0.2° and were found to be always smaller than 10°.

CW–EPR and ENDOR experiments were performed with a Q-band (34 GHz) EPR spectrometer (Bruker ElexSYS E500, equipped with an Oxford CF935 cryostat and an ENDOR system). Angular dependence experiments were carried out at 50K for EPR and in the range 30K-50K for ENDOR, depending on the signal intensities. Simultaneous TL and EPR measurements were performed on K_2YF_5:Tb (0.2%) by connecting the EPR sample holder to an Ocean optics QE65000 spectrometer through a quartz rod and fiber. Sample irradiations were performed at 77K with white radiation from a Philips tungsten anticathode X-ray tube operated at 60 kV and 40 mA, for 20 minutes, corresponding to doses of the order of 20 kGy. Pulse and step annealing experiments were performed by heating the sample in situ to a certain temperature during one hour. In the case of pulse annealing experiments the sample was cooled to 50K for the EPR measurements after each annealing step. In the case of step annealing the EPR measurements were performed at the annealing temperature. In this approach a direct correlation between TL and paramagnetic center bleaching is obtained, eliminating systematic errors when comparing data from separated experiments.[23] Neither approach corresponds to a classical TL experiment, with which the results can thus only be compared in a qualitative way.

III. RESULTS

A. EPR spectrum and thermal bleaching

Figure 1 shows the Q-band EPR spectrum of K_2YF_5: Ce^{3+} (0.2%), recorded at 50K with the magnetic field along the *b* axis, after X-ray irradiation at 77K and rapid transfer of the sample to the spectrometer. It was checked that during the transfer the sample temperature does not rise above 90K. It is clearly seen that X-ray irradiation at 77K temperature produces several paramagnetic defects in the crystal. Prior to irradiation, only the EPR signals of Gd^{3+} are visible at this temperature. From the analysis of the angular dependence of the EPR spectra, at least seven different spectral components can be distinguished, next to

the transitions of Gd^{3+} already present before irradiation. It should also be noted that at this temperature, no RE related EPR spectra, except for S-state ions, are expected to be visible. Five of the radiation-induced spectral components show a strong self HF interaction of the electron spin **S**=1/2 with two nuclei with **I**=1/2 and can be described by the common spin Hamiltonian (SH):

$$\hat{H}_S = \mu_B \vec{B}\cdot\vec{\vec{g}}\cdot\hat{\vec{S}} + \hat{\vec{S}}\cdot\vec{\vec{A}}_1\cdot\hat{\vec{I}}_1 - g_n^F\mu_n\vec{B}\cdot\hat{\vec{I}}_1 + \hat{\vec{S}}\cdot\vec{\vec{A}}_2\cdot\hat{\vec{I}}_2 - g_n^F\mu_n\vec{B}\cdot\hat{\vec{I}}_2 + \sum_i\left(\hat{\vec{S}}\cdot\vec{\vec{A}}_i\cdot\hat{\vec{I}}_i - g_{n,i}\mu_n\vec{B}\cdot\hat{\vec{I}}_i\right) \qquad (1)$$

The last term in Eq. (1) represents superhyperfine (SHF) interactions with surrounding ions that have a nuclear magnetic moment. For all these centers, only interactions with ^{19}F nuclei have been detected. In K_2YF_5, F_2^- centers correspond to trapped hole states.[24-26] The fact that all of them have been detected in crystals doped with Ce^{3+}, Tb^{3+} and Dy^{3+}, as well as in undoped crystals leads us to conclude that they are of intrinsic nature. We labeled them V1-V5 in order of decreasing thermal stability. The integral line intensity of all centers is similar to that of the uncontrolled impurity Gd^{3+}, whose concentration we estimate to be one order of magnitude smaller than the dopant concentration.

In Fig. 2 the results of step annealing experiments for the Ce^{3+} (0.1%) and Tb^{3+} (0.2%) doped crystals are shown, where the symbols represent the intensity of the EPR signals obtained by double integration of the spectra. In these experiments the crystal was kept at a certain temperature during typically one hour while simultaneously recording the EPR and TL spectra. The recording time for EPR measurements was 40 s and accumulation time for luminescence 10 s. The annealing time depended on the processes going on in the crystal, as monitored by EPR/TL. For example, the T=100K annealing was performed until the V3-V5 EPR signals had completely vanished. The TL spectra, shown as insets in Fig. 2, were checked to correspond to the luminescence spectra of the RE activator.[2] The TL response for Ce^{3+} doping is known to be lower than for Tb^{3+} doping, while at the same time the spectrum is much broader (Ce^{3+} (5d→4f) vs. Tb^{3+} (4f→4f)). These are probably the main reasons why the TL was not observable for the Ce^{3+} doped sample, while in Fig. 2(a) four peaks are discernable.

The similarity of the EPR bleaching curves for both crystals is striking: the complete decay of V3-5 at 100K is accompanied by an increase of the intensity for V1. Raising the temperature to 120K leads to a partial decay of V1 and V2, both to about half of their intensity. A first TL glow peak then also occurs. With further rising to 140K, the intensity of the spectrum of V2 decays completely to zero. V1 again loses about half its intensity and a second glow peak is observed. Annealing at 160K produced no new TL peak. V1 completely decays, after which no more F_2^- centers are left in the Tb^{3+} doped crystal. Still, at 180K and close to 300K, two more glow peaks are observed. In the Ce^{3+} doped crystal, the situation is different. The decay of V1 at 160K leads to the production of two closely related F_2^- centers (see also Section III.B.). As more clearly illustrated in Fig. 3 traces of these centers, which we label V1′ and V1″,

are already observable after the decay of V2. V1′ and V1″ only decay close to 300K. From a comparison with the spectra obtained after irradiation at 300K, we conclude that V1″ corresponds to the center produced by 300K irradiation (C4), which was erroneously assumed to be identical to the V1, center produced by irradiation at 77K, in Ref.[17]

Finally, we remark that pulse annealing experiments essentially yielded the same information, explicitly demonstrating that all thermally induced changes in the spectrum are irreversible. The same results were also obtained from experiments on nominally undoped and Dy^{3+} doped crystals, although in some crystals the V2 center was not observed. A more detailed discussion of the origin of the decay of the various centers observed with EPR and the correlation with TL is given in Section IV.B.

B. Angular dependence of spectra and spin Hamiltonian analysis

From the angular dependence of the EPR resonance line positions in three (approximately) perpendicular planes, the g, A_1 and A_2 self HF tensors for the V1-5 centers can in principle be determined. However, in order to obtain high accuracy in these parameters, as needed for structural assignments (see Section IV.A), one should be able to identify not only the outer lines in the spectrum ($M_{I1} = M_{I2} = \pm ½$), but also the central transitions ($M_{I1} = \pm ½$, $M_{I2} = \mp ½$) for several orientations in the three planes. For V1 and V2 this presents no problem, as their spectra can be studied after annealing out V3-5. For the latter centers the situation is obviously more problematic. As a result of low signal intensity and overlap with the other spectral components, only part of the angular dependence of V4 and V5 could be recorded and certain parameters of the corresponding tensors could only be estimated. For V1-3 the spin Hamiltonian parameters could be determined very accurately, as evidenced by the nearly perfect correspondence between experimental and calculated angular dependences in Fig. 4. The open squares represent the experimental data and the solid lines are simulations, using the best fit SH parameters from Table I. For V4 and V5, the estimated parameters are also given. In the following, the general properties of the various centers will be discussed.

In spite of clear misalignments of the crystals, for all magnetic field orientations only two symmetry related sites can be observed for V1 in Fig. 4(a). This demonstrates that it has the same monoclinic symmetry as the YF_7 polyhedra in the structure,[14] i.e. with a mirror plane perpendicular to the c axis. The observed principal A_1, A_2 and g values are very similar to those determined for F_2^- in other fluoride lattices, a selection of which is listed in Table II. In the ENDOR spectra (not shown here), only small couplings with neighboring ^{19}F nuclei are evident.

In a wide angular range, the V2 EPR transitions exhibit, in addition to the HF interactions, also a resolved triplet SHF structure due to two (nearly) equivalent ^{19}F nuclei. This can be seen in Figs. 1 and 4(b). The A3/A4 SHF tensors for the latter nuclei could also be determined (see Table I), albeit with lower accuracy

than those for the central nuclei of the F_2^- molecular anion. No ENDOR was observed for this center, for which the symmetry is again clearly monoclinic. Although not all transitions could be followed throughout the complete angular dependence, it was clearly established that the $g_x \approx g_y$ values for V2 are significantly smaller than for V1 and V3.

In Fig. 4(c) we see that for an arbitrary magnetic field orientation, four symmetry related sets of transitions belonging to V3 are detected. This center thus lacks mirror symmetry. For magnetic field orientations near the *b* axis, its transitions exhibit a partially resolved doublet SHF structure, which could also be detected in the ENDOR spectrum. Its angular dependence in the *ab* plane is shown in Fig. 5. The interactions with two nuclei (tensors A3/A4) are larger than all others and the resolved structure in the EPR spectra corresponds to the larger coupling (A3). As ENDOR data from other planes are lacking, the SHF tensors principal values and directions could not be determined with high accuracy for these interactions. The best-fit results for these tensors are also presented in Table I. We observe that the smaller interaction exhibits a maximum close to the *a* axis, whereas for the larger interaction the maximum is tilted ~20° away from the *b* axis. As explained above, inclusion of the central EPR transitions in the fitting greatly improves the accuracy with which the g, A_1 and A_2 tensors can be determined. For this reason, ENDOR-induced EPR (EIE) experiments were performed for V3, as illustrated in Fig. 6. In the EPR spectrum (top) the central lines of V3 completely overlap with those of V1. Monitoring the intensity of the A4 line marked in the ENDOR spectrum (inset) recorded at one of the outer lines at low field, the EPR spectrum of this symmetry-related orientation of V3 is separated out. In the EIE spectrum the doublet splitting due to the large SHF interaction (A3) is still visible. The negative features in it, appearing at the resonance field positions of V1, are a result of partial overlapping of ENDOR lines. It is interesting to note that, due to large second order corrections to the ENDOR frequencies as a result of the strong coupling to the central ^{19}F nuclei (A1/A2),[27, pp.188-194] the EPR spectrum is not completely reconstructed when recording the EIE spectrum at the transitions corresponding to the larger A3 coupling.

IV. DISCUSSION

A. Nature and location of centers

As already mentioned, comparison of the spin Hamiltonian data in Table I with literature data in Table II leaves little doubt that all centers V1-5 have the F_2^- molecular anion as core. X_2^- centers (X = F, Cl, Br, I) in alkali halides and perovskites have nearly axial symmetry and theoretical analysis of their electronic ground state has demonstrated that their X–X axis coincides with the principal g direction corresponding to the smallest principal value ($g_z \approx g_e$). The unpaired electron indeed resides mainly in the p_z-lobes of the

F-atoms constituting the molecular ion. The axes along which the largest principal values of A_1 and A_2 are found, are also very close to this direction. Usually, a distinction is made between V-type centers, in which a hole is shared between two lattice X^- ions, and H-type centers involving a lattice and an interstitial anion. Literature data on these types of centers indicate that the (positive) shift from the free electron value of $g_x \approx g_y$ for a V-type center is about twice as large as for an H-type,[28] as can be seen in Table II. In the following, we determine the nature and lattice location of V1-3, mainly based on a comparison of their principal g and A directions with bond directions in the undistorted K_2YF_5 lattice. In addition, the monoclinic symmetry of V1 and V2 suggests that they are situated in the mirror plane of the YF_7 polyhedron, whereas V3 should be tilted outside of this plane. Fig. 7 shows the most plausible models for these three centers.

For V1, and also for V1′ and V1″, the deviation between the principal g_z and F4–F5 bond direction is less than 1° (see Fig. 7(a)). The model also explains why no large HF interactions with neighboring ^{19}F ions have been detected in the ENDOR spectra of V1. None of the nearby F^- ions are situated close to the F–F bond axis of the center, so their HF tensors are expected to have only small contributions from direct overlap. In view of its abundant formation at low temperatures, the V1 center most probably is a V_K center, i.e. a hole trapped between two nearest neighbor lattice anions in an otherwise undisturbed lattice. The lower crystal symmetry of K_2YF_5, as compared to alkali halides and perovskites, explains why even in this simple, purely intrinsic defect the symmetry is lower than axial and why the two ^{19}F ions are not exactly equivalent. Although little information from experiment is available to establish the nature of the difference with V1, analogy with the situation in alkali halides makes us believe that V1′ and V1″ might be V_F or V_{KA} centers, involving a nearby cation vacancy or impurity.[29] Finally, from the thermal bleaching study we derive that F4–F5 is by far the most stable position in the lattice for intrinsic hole trapping.

In the case of V2 the additional SHF interaction with two (nearly) equivalent neighboring fluorine ions, that produces the additional splitting of the EPR lines, also has to be taken into account. All principal tensor axes for this center are found to be tilted about 20° away from the b axis. As shown in Fig. 7(b), an H center on the position F3 is the most plausible structure giving rise to this set of interactions. It is worth noting that F3 was also found to be the most plausible lattice location for the most stable trapped hole center C1 in $K_2YF_5:Ce^{3+}$ after irradiation at 300K, which is most probably oxygen-related (O_2^-).[18] The fact that its $g_x \approx g_y$ shifts are found to be significantly lower than for V1 and V3 seems to support the identification as an H center. The triplet SHF structure only rarely appears in the 1:2:1 intensity ratio characteristic for two nuclei with equal coupling strength, so the ions causing it (see Fig. 7(b)) are not

expected to be exactly equivalent. As we observed no ENDOR for this center, their inequivalence could, however, not be firmly established.

Finding the lattice position for the triclinic V3 center is less evident. Its $g_x \approx g_y$ shifts suggest that it is a V_K center. Restricting the model space to nearest neighbor F^- ions in the same YF_7 polyhedron, six positions for hole trapping with triclinic symmetry are to be considered : F5–F2/6, F3–F2/6, F4–F1/7, F4–F2/6, F3–F1/7, and F1/7–F2/6. Based on the orientation of the principal g, A_1 and A_2 directions, the latter three positions can immediately be discarded. Considering also the SHF interactions observed in ENDOR, the most plausible position for this center is F5–F2/6, as presented in Fig. 7(c). The largest of the SHF interactions would then be caused by an ion along the F–F bond axis, next to F2/F6, in the neighboring YF_7 polyhedron along the chain, as shown in Fig. 7(d). Based on the direction of the main symmetry axis of A4, the second largest SHF interaction can be attributed either to F4 or to an F^- ion in the symmetry-related chain. These are marked with an asterisk in Fig. 7(c). ENDOR experiments in a second, perpendicular rotation plane can in principle distinguish between these two cases, but were unsuccessful in our case.

The spin Hamiltonian parameters for V4 and V5 have insufficient accuracy, especially with regard to the principal tensor axes, to allow model assignations. For V4, the monoclinic symmetry suggests a position in the mirror plane of the YF_7 polyhedron. Its $g_x \approx g_y$ shifts are indicative of a V_K model, but F4–F5 is the only position for hole trapping with mirror symmetry, and the principal directions of V4 and V1 are largely different. For V5, the triclinic symmetry and the similarity in g_z and A_z directions to V3 suggest that a V_K center between lattice positions F3–F2/6 or F4–F1/7 might be a good model.

B. Stability and relation with TL below 300K

Both V- and H-type F_2^- centers, are trapped hole states in the K_2YF_5 lattice. All TL signals below 300K exhibit the characteristics of a RE^{3+} luminescence spectrum (see insets Fig. 2). Hence, direct radiative recombination of an electron at the trapped hole F_2^- centers can be immediately discarded as TL mechanism. Only two processes can then still be considered in which F_2^- centers may play a direct role in the TL. The first possibility involves the spontaneous or characteristic decay of the F_2^- centers, i.e. via release of the trapped hole to the valence band or thermally activated motion of the trapped state, and recombination with a still trapped electron. In the second, thermally released electrons recombine at the F_2^- center and the recombination energy is transferred to a nearby activator center. For the trapped hole centers this type of decay may be labeled as induced. Spontaneous decay at a certain temperature is expected to be complete and independent of dopants in the crystal. Induced decay, on the other hand, may be partial and may be expected to have a similar effect on trapped hole centers of similar nature (and

comparable trapping cross section). It may be dependent of the RE-doping if the trapped electron states are influenced by it. Further experimental information about the origin of the decay for the various centers may be obtained in photo-EPR experiments, in which only effects caused by transfer of trapped charges are expected to be observed, allowing to make the distinction with other, thermally induced structural changes, e.g. vacancy or interstitial motion. Such experiments were not attempted here.

Bearing this in mind, we reconsider the EPR thermal bleaching experiments and correlated TL measurements in Fig. 2. At 100K for both types of RE-doping, the spontaneous decay of V3-V5 into V1 is observed. Indeed, the increase in intensity for the V1 center roughly corresponds to the cumulated intensity of V3, V4 and V5 before annealing. It should further be noted that the decay of V3-V5 is not accompanied by a TL signal, which suggests a complete transfer of the trapped charges to the deeper trap, without (partial) recombination with trapped electrons.

The partial decay to roughly half intensity of V1 and V2 at 120K is clearly induced. As it is observed in all crystals studied so far, the trap from which electrons are released is most probably intrinsic. At this temperature, a TL peak was observed in Tb^{3+} crystal. The complete decay of the V2 center at 140K in both crystals points to spontaneous decay, whereas the simultaneous decay of V1 is clearly induced, and indicates that also an intrinsic electron trap is emptied at this temperature. Also here a TL peak occurs. At 160K the spontaneous decay of V1 is observed both in Ce^{3+} and in Tb^{3+} doped crystals. This decay is again not marked by a TL signal.

In Ce^{3+} doped crystals, part of the holes released from V2 and V1 get trapped at two centers closely related to V1, having much higher thermal stability, though. The spontaneous decay time of V1″=C4 has been determined as ~2 h at 300K.[17] The fact that these centers are not observed in Tb^{3+} doped crystals might indicate that they are Ce^{3+}-related and/or that in Tb^{3+} doped crystals other hole traps are more efficient or abundant. The occurrence in these crystals of two more TL peaks when all F_2^- centers have already decayed is an indication for the latter explanation.

These observations strongly indicate that for none of the observed TL peaks, hole release from an F_2^- type center and subsequent recombination with a trapped electron is an adequate mechanism. On the contrary, thermally induced electron release appears to initiate the TL observed at 120 and 140K. In Fig. 8, the negative derivative of the V1 and V2 EPR intensities are compared with the TL intensity in the temperature ranges of decay. A very good correlation is found between the decay of V1 and the TL intensities. This indicates that recombination at V1 and energy transfer to a nearby activator center might be appropriate mechanisms to explain the occurrence of the glow peaks at 120K and 140K. A similar mechanism involving V2 cannot be excluded : although the correlation between the thermal bleaching of

this center and the TL intensity of the two peaks is less obvious, it should be borne in mind that at 140K the evolution of the V2 EPR spectrum is at least in part due to TL-free spontaneous decay.

The close correspondence between the two curves in Fig. 8 does, however, by no means, serve as a direct proof of the involvement of V1 in the two related TL peaks. Indeed, all decay processes of trapped hole centers induced by the thermal release of electrons from a certain trap, and hence in particular also the TL, may be expected to be proportional. The possibility that V1 and V2 do not play a direct role in the TL at 120 and 140K but only act as observers of the thermal release of electrons cannot be excluded at this moment. They then have a negative influence on the TL efficiency at these temperatures. In that case, the as yet unobserved trapped hole centers might, e.g., be activator-related, as suggested in earlier TL studies on these materials.[2] As, except for Gd^{3+}, the RE-related EPR spectra were not monitored in this study (their spectrum is not visible at the measurement temperatures), we have obtained no information about RE activator and/or impurity ions in carrier trapping processes. In this context, it should be noted that we earlier established that no RE-related EPR spectra are produced in $K_2YF_5:Tb^{3+}$ upon irradiation at 77K, but that subsequent anneal to 300K leads to strongly angular dependent EPR signals in a wide magnetic field range,[17] typical for RE-related paramagnetic centers. A more systematic study of the thermal production and decay of these signals will provide further information concerning the role of V1 and V2 in the TL peaks at 140 and 160K, and may possibly also provide an explanation for the occurrence of the glow peaks above 160K in $K_2YF_5:Tb^{3+}$.

V. CONCLUSIONS

X-ray irradiation at 77K of K_2YF_5:RE crystals leads to the production of a wide variety of intrinsic trapped hole centers of the F_2^--type. Two of them are more stable than the others: V1, identified as a V_K-type center between the fluoride lattice positions F4 and F5, and V2, an H-type center at position F3. Already at 100K, three other F_2^- centers irreversibly transform into V1. One of them, V3, exhibiting triclinic symmetry is most probably located at F5–F2/6. Simultaneous EPR thermal bleaching and TL experiments suggest that V1 and V2 might be directly involved in two glow peaks occurring at 120K and 140K as recombination centers for thermally released electrons. At 160K, the holes trapped at V1 become mobile and are transferred to deeper traps. In Ce^{3+} doped crystals, two of those, V1′ and V1″ are structurally very similar to V1 and also located at F4–F5, whereas in Tb^{3+} doped crystals these trapped hole states remain as yet unidentified. A thorough study of the evolution of RE-related EPR spectra at lower temperatures might further clarify this situation, in particular with respect to the possible function of activator centers as hole traps.

VI. ACKNOWLEDGEMENTS

The authors acknowledge the Flemish Research Foundation (FWO-Vlaanderen) for financially supporting this work (Grant no. G.0116.06N). H. Vrielinck and P. F. Smet acknowledge a Postdoctoral Fellowship with the same institution. We would also like to thank prof. N. M. Khaidukov (Institute of General and Inorganic Chemistry, Russian Academy of Sciences) for crystal growth and helpful discussions about their structural properties.

VII. REFERENCES

[1] L. O. Faria, D. Lo, H. W. Kui, N. M. Khaidukov, and M. S. Nogueira, Radiat. Prot. Dosim. **112**, 435 (2004).
[2] H. W. Kui, D. Lo, Y. C. Tsang, N. M. Khaidukov, and V. N. Makhov, J. Lumin. **117**, 29 (2006).
[3] J. Marcazzo, M. Santiago, E. Caselli, N. Nariyama, and N. M. Khaidukov, Opt. Mater. **26**, 65 (2004).
[4] J. A. Nieto, N. M. Khaidukov, C. B. Guerrero, J. C. A. Vega, T. R. Montalvo, A. G. Cuellar, J. Gongora, and P. R. G. Martinez, Rad. Eff. Defect. S. **161**, 443 (2006).
[5] M. S. Rasheedy, M. A. El-Sherif, and M. A. Hefni, Rad. Eff. Defect. S. **161**, 579 (2006).
[6] E. C. Silva, N. M. Khaidukov, M. S. Nogueira, and L. O. Faria, Radiat. Meas. **42**, 311 (2007).
[7] D. McLean, J. Varas, and N. Khaidukov, Radiat. Phys. Chem. **71**, 995 (2004).
[8] P. Dorenbos, R. Visser, C. W. E. Vaneijk, N. M. Khaidukov, and M. V. Korzhik, IEEE T. Nucl. Sci. **40**, 388 (1993).
[9] P. Dorenbos, R. Visser, C. W. E. Vaneijk, J. Valbis, and N. M. Khaidukov, IEEE T. Nucl. Sci. **39**, 506 (1992).
[10] A. Yoshikawa, K. Kamada, M. Nikl, K. Aoki, H. Sato, J. Pejchal, and T. Fukuda, J. Cryst. Growth **285**, 445 (2005).
[11] J.-M. Spaeth, J. R. Niklas, and R. H. Bartram, *Structural analysis of point defects in solids : an introduction to multiple magnetic resonance spectroscopy* (Springer-Verlag, Berlin ; New York, 1992).
[12] V. V. Laguta, M. Martini, A. Vedda, E. Rosetta, M. Nikl, E. Mihokova, J. Rosa, and Y. Usuki, Phys. Rev. B **67**, 205102 (2003).
[13] V. V. Laguta, M. Nikl, and S. Zazubovich, IEEE T. Nucl. Sci. **55**, 1275 (2008).
[14] F. Loncke, D. Zverev, H. Vrielinck, N. M. Khaidukov, P. Matthys, and F. Callens, Phys. Rev. B **75**, 144427 (2007).
[15] K. Gude and C. Hebecker, Z. Naturforsch. B **40**, 864 (1985).
[16] Y. A. Kharitonov, Y. A. Gorbunov, and B. A. Maximov, Kristallografiya **28**, 1031 (1983).
[17] H. Vrielinck, D. Zverev, P. F. Smet, D. Poelman, T. Gregorkiewicz, and F. Callens, Mat. Sci. Eng. B-Solid **146**, 16 (2008).
[18] D. Zverev, H. Vrielinck, F. Callens, P. Matthys, S. Doorslaer, and N. M. Khaidukov, Phys. Chem. Chem. Phys. **10**, 1789 (2008).
[19] M. A. Dubinskii, N. M. Khaidukov, I. G. Garipov, L. N. Demyanets, A. K. Naumov, V. V. Semashko, and V. A. Malyusov, J. Mod. Optic. **37**, 1355 (1990).
[20] S. L. Baldochi, L. C. Courrol, R. E. Samad, I. M. Ranieri, L. Gomes, A. Z. de Freitas, and N. D. Vieira, Phys. Status Solidi C **4**, 1060 (2007).
[21] T. G. Stoebe and L. A. Dewerd, J. Appl. Phys. **57**, 2217 (1985).
[22] A. N. Yazici, V. E. Kafadar, and H. Toktamis, Nucl. Instrum. Meth. B **246**, 387 (2006).
[23] A. Ege, Y. Wang, and P. D. Townsend, Nucl. Instrum. Meth. A **576**, 411 (2007).

[24] L. E. Halliburton, A. Jafari, and R. A. Burris, Phys. Rev. B **23**, 6765 (1981).
[25] B. H. Rose, J. E. Rhoads, and L. E. Halliburton, Phys. Rev. B **14**, 3583 (1976).
[26] L. J. Vande Kieft and O. R. Gilliam, Phys. Rev. B **1**, 2015 (1970).
[27] N. M. Atherton, *Principles of electron spin resonance* (Ellis Horwood ; PTR Prentice Hall, New York, 1993).
[28] I. Tale, M. Springis, U. Rogulis, V. Ogorodnik, P. Kulis, V. Tale, A. Veispals, and H. J. Fitting, Radiat. Meas. **33**, 751 (2001).
[29] Schoemak.D, Phys. Rev. B **7**, 786 (1973).
[30] T. P. P. Hall, Br. J. Appl. Phys. **17**, 1011 (1966).
[31] L. E. Halliburton and E. Sonder, Solid State Commun. **21**, 445 (1977).
[32] W. Kanzig, J. Phys. Chem. Solids **17**, 80 (1960).
[33] T. G. Castner and W. Kanzig, J. Phys. Chem. Solids **3**, 178 (1957).
[34] W. Kanzig and T. O. Woodruff, J. Phys. Chem. Solids **9**, 70 (1958).

Table I. EPR parameters

		Direction cosines, *abc* ref. frame		
	g			
	2.0193^{+6}_{-9}	0	0	-1
V1	2.0201^{+5}_{-11}	0.587	0.809	0
	2.0013^{+6}_{-10}	0.809	-0.587	0
	A_1 (MHz)			
	152^{+67}_{-85}	0	0	-1
	150^{+87}_{-101}	0.643	0.766	0
	2464^{+16}_{-21}	0.766	-0.643	0
	A_2 (MHz)			
	215^{+73}_{-70}	0	0	-1
	202^{+106}_{-60}	0.545	0.839	0
	2552^{+25}_{-14}	0.839	-0.545	0
	g			
	–	0	0	-1
V1′	2.0184^{+5}_{-15}	0.586	0.810	0
	2.0014^{+7}_{-15}	0.810	-0.586	0
	A_1 (MHz)			
	–	0	0	-1
	<200	0.578	0.816	0
	2528^{+40}_{-40}	0.816	-0.578	0
	A_2 (MHz)			
	–	0	0	-1
	<200	0.647	0.763	0
	2528^{+39}_{-39}	0.763	-0.647	0
	g			
	–	0	0	-1
V1″=C4	2.0200^{+8}_{-8}	0.588	0.809	0
	2.0014^{+7}_{-7}	0.809	-0.588	0
	A_1 (MHz)			
	–	0	0	-1
	101^{+97}_{-294}	0.621	0.784	0
	2460^{+20}_{-20}	0.784	-0.621	0
	A_2 (MHz)			
	–	0	0	-1
	202^{+72}_{-470}	0.580	0.814	0
	2602^{+20}_{-20}	0.814	-0.580	0

	g			
	2.0152^{+11}_{-13}	0	0	-1
V2	2.0152^{+13}_{-13}	0.820	0.572	0
	2.0012^{+10}_{-10}	0.572	-0.820	0
	A_1 (MHz)			
	<200	0	0	-1
	<200	0.775	0.632	0
	2668^{+25}_{-32}	0.632	-0.775	0
	A_2 (MHz)			
	<200	0	0	-1
	<200	0.851	0.508	0
	2488^{+23}_{-32}	0.508	-0.861	0
	A_3/A_4 (MHz)			
	0	0	0	-1
	0	0.807	0.590	0
	79^{+3}_{-14}	0.590	-0.807	0
	g			
	2.0216^{+21}_{-20}	-0.501	0.742	-0.445
V3	2.0225^{+20}_{-21}	-0.832	-0.270	0.485
	2.0011^{+15}_{-15}	0.240	0.613	0.753
	A_1 (MHz)			
	<200	-0.764	0.582	-0.278
	<200	-0.592	-0.461	0.661
	2351^{+40}_{-38}	0.257	0.670	0.697
	A_2 (MHz)			
	<200	-0.594	0.738	-0.318
	<200	-0.767	-0.400	0.502
	2702^{+40}_{-38}	0.243	0.542	0.804
	A_3 (MHz)			
	<0.5	0.227	0.553	-0.802
	<0.5	-0.925	0.379	0
	40.2^{+13}_{-7}	0.304	0.742	0.598
	A_4 (MHz)			
	<0.5	0.338	-0.394	-0.855
	<0.5	-0.759	-0.651	0
	8.8^{+6}_{-6}	-0.557	0.648	-0.519
	g			
	2.0200^{+10}_{-9}	0	0	-1
V4	2.0204^{+14}_{-15}	-0.987	-0.163	0
	2.0015^{+4}_{-6}	-0.163	0.987	0
	A_1 (MHz)			
	<200	0	0	-1

	<200	-0.992	-0.128	0
	2595^{+15}_{-15}	-0.128	0.992	0
	A_2 (MHz)			
	<200	0	0	-1
	<200	-0.977	-0.213	0
	2427^{+17}_{-14}	-0.213	0.977	0
	g			
	2.0235^{+17}_{-19}	0.455	0.471	-0.756
V5	2.0211^{+10}_{-12}	-0.834	0.523	-0.176
	2.0014^{+12}_{-13}	0.313	0.710	0.631
	A_1/A_2 (MHz)			
	<200	0.455	0.471	-0.756
	<200	-0.834	0.523	-0.176
	2466^{+23}_{-35}	0.313	0.710	0.631

Table II. Spin Hamiltonian parameters of F_2^- centers in different lattices.

Type of the center	g_x	g_y	g_z	Ref.
H in $RbCaF_3$	2.0133	2.0133	2.0023	[24]
H in $KMgF_3$	2.0140	2.0125	2.0032	[25]
F_2^- in NH_4HF_2	2.0152	2.0152	1.9998	[26]
F_2^- in $NaHF_2$	2.0158	2.0158	2.0001	[26]
V_K in $LiBaF_3$	2.024	2.024	2.002	[28]
V_K in $CsCaF_3$	2.0244	2.0244	2.0031	[28]
V_K in $KMgF_3$	2.021	2.021	2.0024	[30]
F_2^- in $KMgF_3$	2.018	2.024	2.0024	[30]
V_K in $RbCaF_3$	2.023	2.023	2.003	[31]
V_F in LiF	2.023	2.023	2.001	[32]
V_K in LiF	2.0227	2.0234	2.0031	[33]
H in LiF	2.014	2.012	2.001	[34]

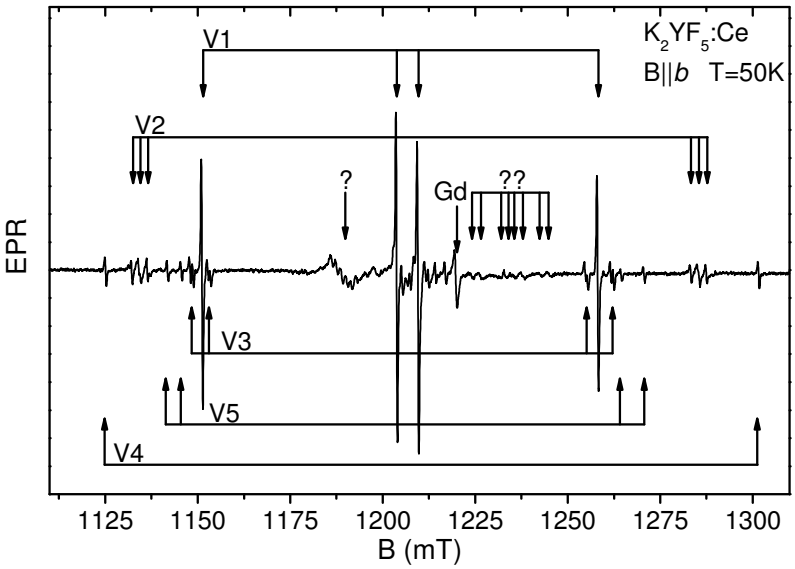

Fig. 1. Q-band EPR spectrum of K_2YF_5:Ce (0.2%) after X-ray irradiation at T=77K.

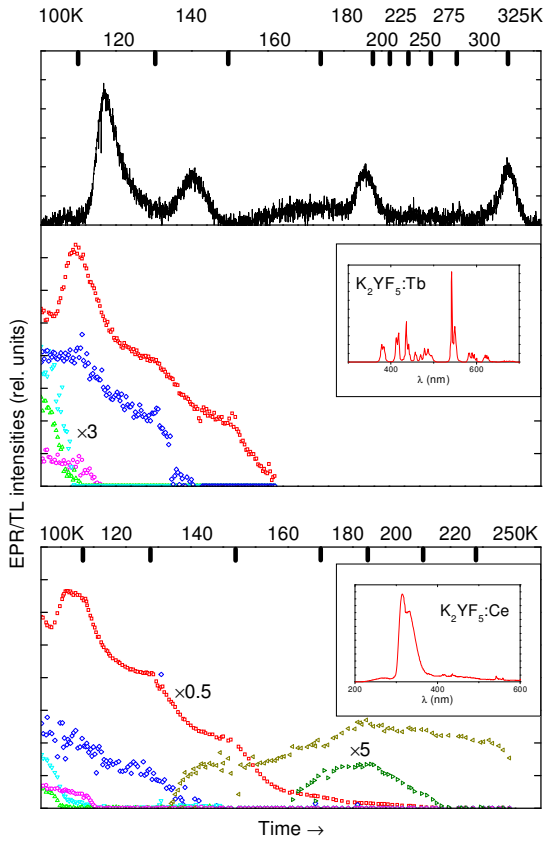

Fig. 2. Step annealing of K_2YF_5:Tb (top) and K_2YF_5:Ce (bottom) irradiated with X-rays at 77K. Symbols correspond to the EPR intensities of F_2^- centers (□ – V1, ◇ – V2, ▽ – V3, △ – V4, ⬡ – V5, ◁ – V1′ and ▷ – C4=V1″). The TL intensity of the KYF:Tb crystal is presented as the solid line

above the EPR intensities. The insets show the corresponding TL spectra observed during rapid annealing of the samples. As indicated, in the top figure the EPR line intensities for centers V3-V5 are multiplied by factor of 3 and in the bottom figure the intensity of V1 is multiplied by 0.5 and of V1′ and V″ by 5.

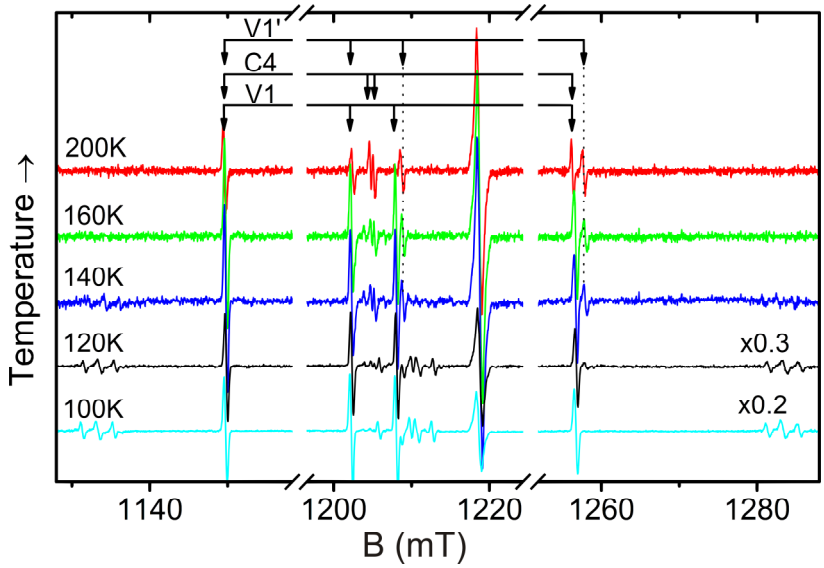

Fig. 3. Transformation of the V1 center into the V1′ and C4 centers with increasing temperature.

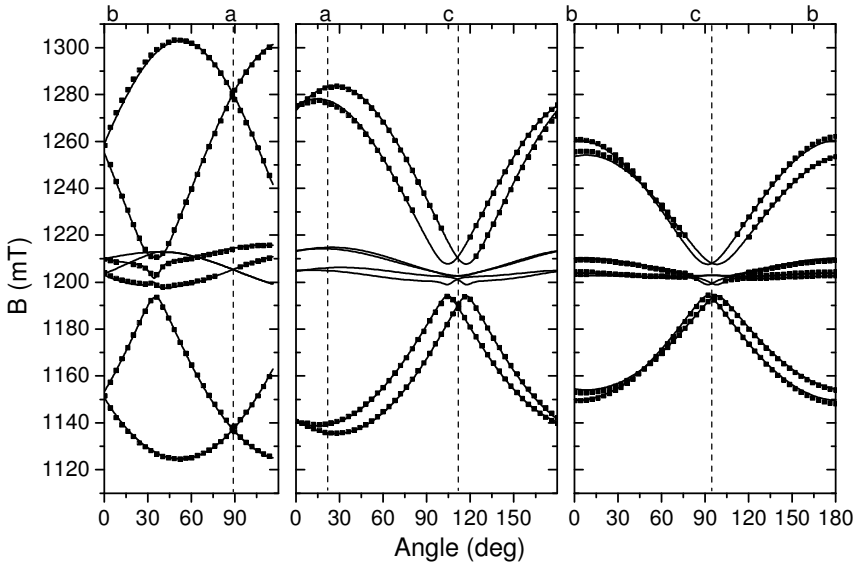

Fig. 4(a). Angular dependence of the V1 EPR resonance positions in the *ab*, *ac* and *bc* planes. The symbols and solid lines correspond to the experimental and calculated resonance positions respectively (parameters from Table I).

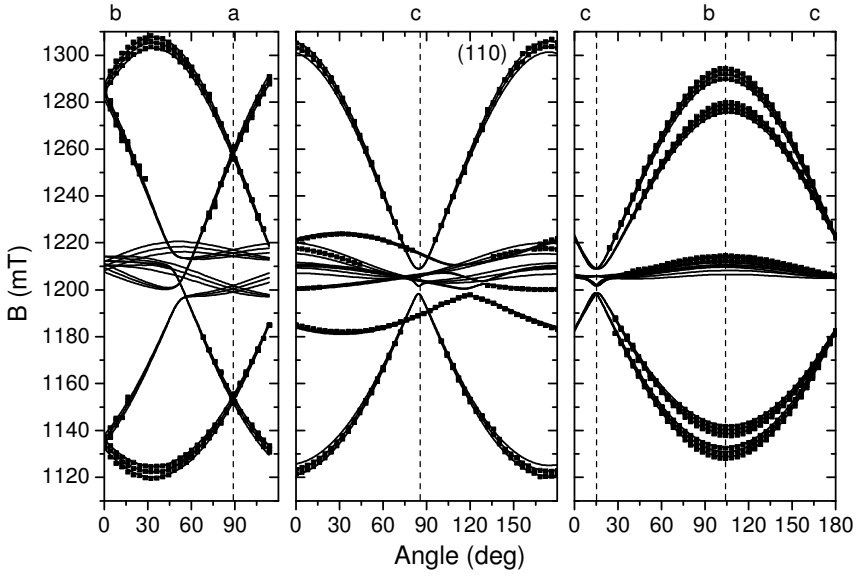

Fig. 4(b). Angular dependence of the V2 EPR resonance positions in *ab*, (110) and *bc* planes. Symbols correspond to the observed resonance positions and lines are the simulation using parameters from Table I.

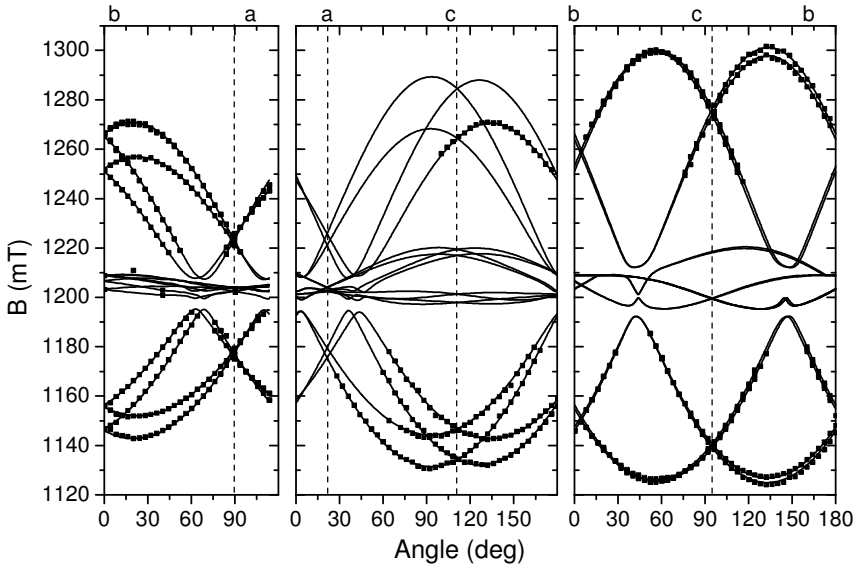

Fig. 4(c). Angular dependence of the V3 EPR resonance positions in *ab*, *ac* and *bc* planes. Symbols correspond to the observed resonance positions and lines are the simulation using parameters from Table I.

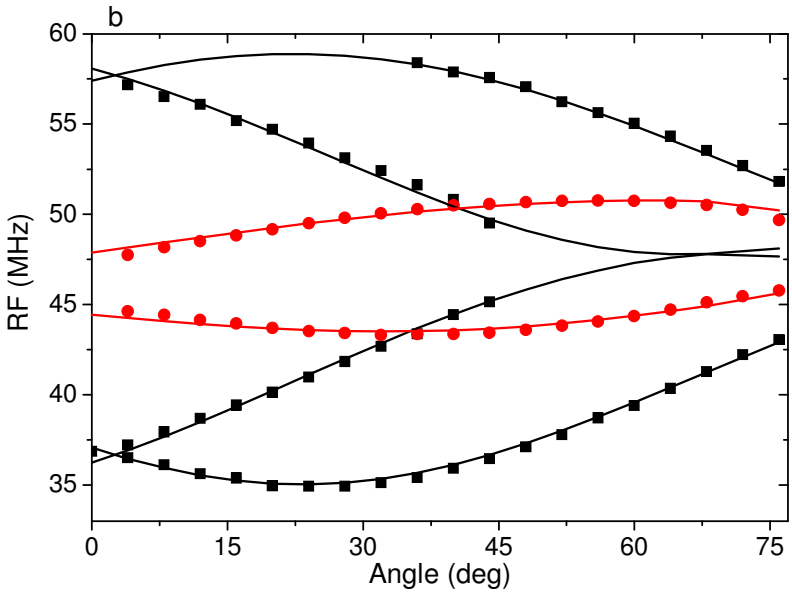

Fig. 5. Angular dependence of the V3 ENDOR resonance positions in the *ab* plane. The symbols correspond to the observed interactions with two different ^{19}F nuclei (A_3 and A_4) and the solid lines are simulations using parameters from Table I.

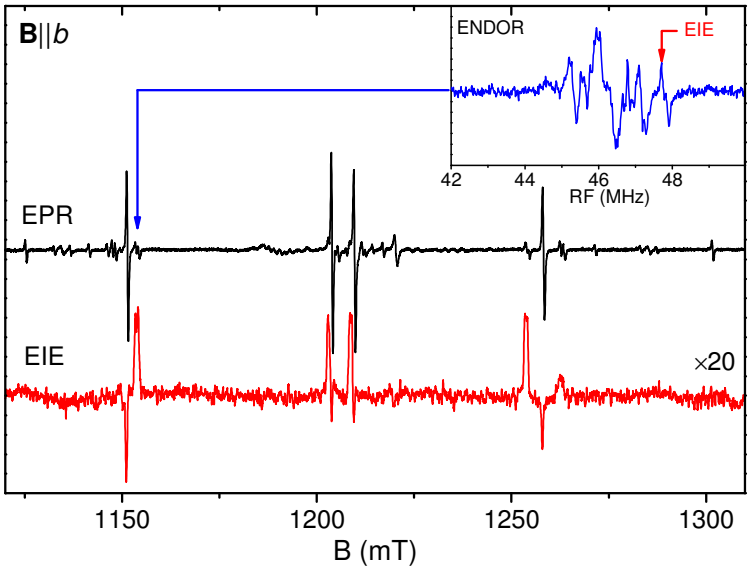

Fig. 6. EPR spectrum of K_2YF_5:Ce, after X-ray irradiation at T=77K (top) and the EIE spectrum corresponding to $\mathbf{B_0}$=1153.8 mT and ENDOR frequency RF_0=47.71 MHz (V3 – center, A_4 interaction) (bottom). The inset depicts the ENDOR spectrum with $\mathbf{B_0}$=1153.8 mT.

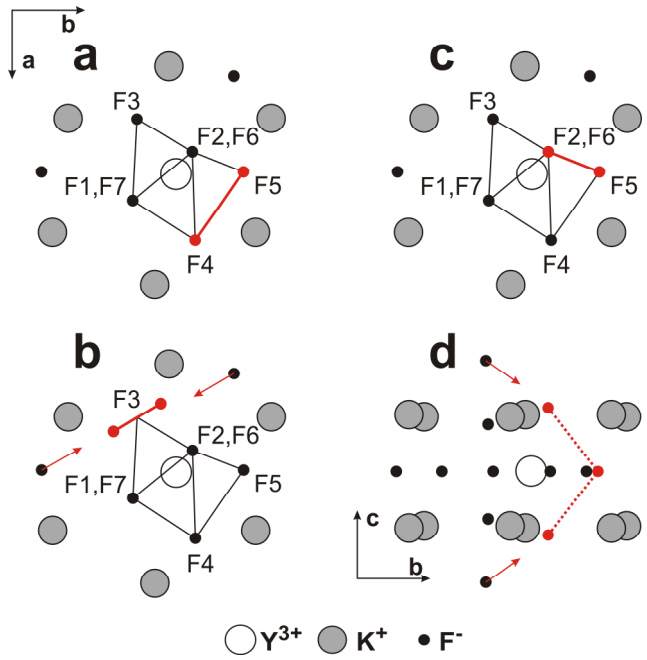

Fig. 7. Possible models of F_2^--centers in K_2YF_5 (**a** – V1 (V_K), **b** – V2 (H), **c** and **d** – V3 (V_K))

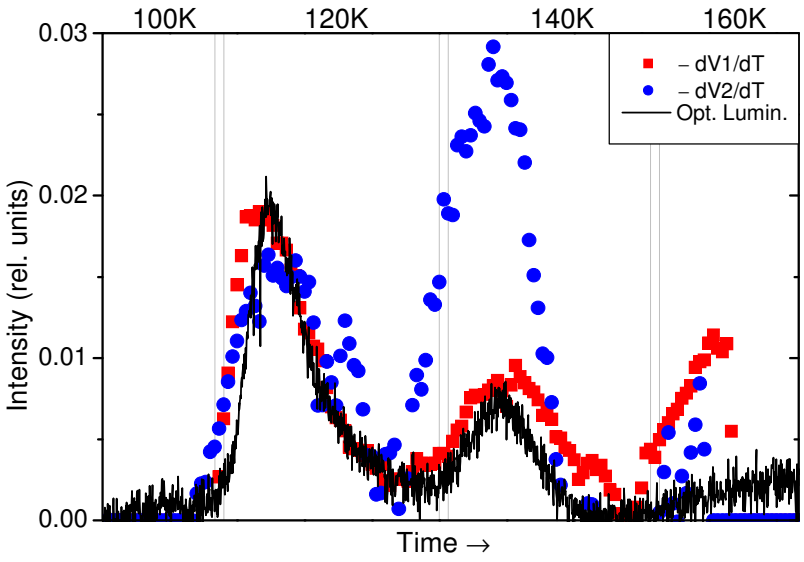

Fig. 8. Negative derivatives –dV1/dT (■) and –dV2/dT (●) of V1 and V2 intensities in K_2YF_5:Tb. The solid line corresponds to the TL of the Tb^{3+} ions.